A MINERAL SCALE GEOCHEMICAL INVESTIGATION OF ULTRAMAFIC ROCKS FROM THE SAN CARLOS AND KILBOURNE HOLE XENOLITH LOCALITIES, SOUTHWESTERN U.S.A.; INSIGHTS INTO THE ORIGIN OF THE REGIONAL SHALLOW MANTLE

ADRIANA M. STOICA[1,2], MIHAI N. DUCEA[1,2]

[1]Faculty of Geology and Geophysics, University of Bucharest, 010041, Bucharest, Romania
[2]University of Arizona, Department of Geosciences, Tucson, AZ 85721, USA
*Corresponding author: ducea@arizona.edu

Abstract. Twenty-one ultramafic xenoliths from the Quaternary San Carlos, Arizona and Kilbourne Hole, New Mexico localities were investigated petrographically. We conducted a series of mineral scale analyses of major and trace elemental chemistry via electron microprobe and laser ablation ICP-MS techniques. Samples comprise various peridotites and pyroxenites derived from the shallowest mantle beneath the modern western U.S.A. region. Peridotites are interpreted to represent the primary depleted shallowest mantle lithospheric rocks of the region, whereas clinopyroxenites, websterites and wehrlites are former melts or cumulate of mafic melts that enriched and/or metasomatized the mantle at some unknown time. Both suites equilibrated at around 1000–1110^0 C and 0.9–1.5 GPa, corresponding to depths of 30–50 km beneath the surface, immediately beneath the modern Moho. Trace elemental concentrations, Mg# and other depletion indicators in peridotites are inconsistent with an (accreted) oceanic plate (Farallon) origin for these rock suites. Instead, they represent a melt-modified native North American depleted mantle lithosphere. We show that to a first order, differences in chemistry between cores and rims of various lithologies are minuscule, lacking diffusional profiles. The implication is that most metasomatic processes that enriched the mantle there are recent, Mesozoic or younger.

Keywords: ultramafic, western U.S.A., mantle lithosphere, thermobarometry.

Résumé. Nous avons étudié pétrographiquement vingt et un xénolites ultramafiques issus des gisements quaternaires de San Carlos (en Arizona) et de Kilbourne Hole (au Nouveau Mexique). Des analyses minérales in situ en éléments majeurs et traces ont été réalisées par microsonde électronique et LA-ICP-MS, respectivement. Ces échantillons consistent en une large variété de péridotites et de pyroxénites issues de la partie supérieure du manteau lithosphérique sous l'actuel région Ouest des États-Unis. Les péridotites sont interprétées comme des reliques originellement appauvries issues de la partie supérieure de la lithosphère, alors que les clinopyroxénites, webstérites et les wherlites sont interprétées comme d'anciens liquides magmatiques ou des unités cumulatives formées à partir de ces mêmes liquides mafiques, ayant enrichi et/ou métasomatisé cette portion du manteau. Les deux assemblages lithologiques se sont équilibrés à des conditions de température autour de 1000–1110°C et de pression avoisinant les 0.9 à 1.5 GPa. Ces conditions correspondent à une profondeur de 30 à 50 km, juste en dessous du Moho moderne. La signature géochimique des péridotites en éléments en trace, en Mg# et d'autres indicateurs d'appauvrissement suggèrent que ces unités ne sont pas liées génétiquement à l'accrétion d'une plaque océanique (Farallon). A contrario, ces roches représentent des vestiges appauvris du manteau lithosphérique nord-américain ayant partiellement été modifiés par la présence de liquides magmatiques. Notre étude démontre que les différences géochimiques entre les cœurs et les bordures des différents échantillons lithologiques sont minimes et exemptes de profils de diffusion. Cela implique que la plupart des processus métasomatiques ayant enrichi le manteau sont relativement récents, probablement mésozoïques.

Mots-clés: ultramafique, ouest-américain, manteau lithosphérique, thermobarométrie.

1. INTRODUCTION

Mineral scale geochemical and isotopic investigations represent the gold standard of unraveling continental upper mantle origin and evolution, as revealed through xenoliths found in basaltic rocks. The great majority of such xenoliths are fragments of the mantle lithosphere. Tools based on major and trace elemental chemistry include thermobarometry, the ability to estimate how depleted a mantle fragment is and therefore how likely it is to belong to a former oceanic domain (Luffi *et al.*, 2009, Quinn *et al.*, 2018) or the continental mantle. The ability to actually date (i.e., obtain a radiometric age of) the extraction of a mantle fragment from the convective mantle is more restricted and is based on the opportunistic application of certain isotopic systems, such as Re-Os depletion ages. Still, a tremendous amount of information can be obtained based on chemical information alone, especially if performed *in-situ*, within grain. Electron microprobe techniques have allowed the determination of major elemental concentrations on ultramafic minerals for decades. The advent of laser ablation single collector ICP-MS techniques in recent years allowed for complementary studies of trace (as well as major) elemental concentrations to be carried out in such materials.

Here we present new mineral chemistry data on various ultramafic xenoliths from Quaternary basaltic rocks from San Carlos (Arizona) and Kilbourne Hole (New Mexico). Both are classic locations (Frey, Prinz, 1978; Wilshire *et al.*, 1988) in the geologic literature. Materials from these locations have been used as standards for various geochemical materials over the past five decades and the xenolith occurrences are famous for richness in material and size of xenoliths. Despite these features, petrologic studies of both localities are somewhat antiquated and numerous petrologic and tectonic questions still linger about the origin of these rocks. For example, it is still a matter of debate as to whether they represent native North American lithospheric fragments or subducted-accreted Farallon materials. Another issue of debate is whether the abundant signs of metasomatic re-fertilization (via passage of melts) seen in these rocks are young extensional features (syn- basaltic magmatism), relatively young subduction-related Cordilleran features (35–200 Ma) or inherited from a previous Wilson cycle.

We address some of these questions in this preliminary petrologic study using major and trace elemental chemistry on all principal ultramafic lithologies from these iconic locations. A subsequent study focusing on radiogenic and stable isotopic systems will complement the findings presented here.

2. PETROGRAPHY

We studied 21 peridotite and pyroxenite xenoliths from the San Carlos and Kilbourne Hole localities (Fig. 1). The peridotite suite of samples investigated includes 14 spinel lherzolites and 2 spinel wehrlites, while the pyroxenite suite is represented by 5 olivine websterites. The sampling at both locations was carried out so that the petrographic and textural variety of the samples recovered (estimated visually in the field) is the most representative for each location, according to previous investigations (Frey, Prinz, 1978; Dromgoole, Pasteris, 1987; Wilshire *et al.*, 1988).

San Carlos samples used for this study (n=10) are olivine-rich spinel lherzolites (n=6), spinel-bearing olivine websterites (n=3), and spinel wehrlite (n=1) (Fig. 2). The majority of samples collected from this location can be classified as Group I, according to the terminology of Frey, Prinz (1978). They have Cr-rich clinopyroxenes and spinels and high forsterite content in olivines (Fo>86). The olivine wehrlite sample (SC07) is the only Group II xenolith used in this study. It has Fe-rich olivines (Fo_{71}), Ti-rich clinopyroxenes, and Al- and Fe-rich spinels.

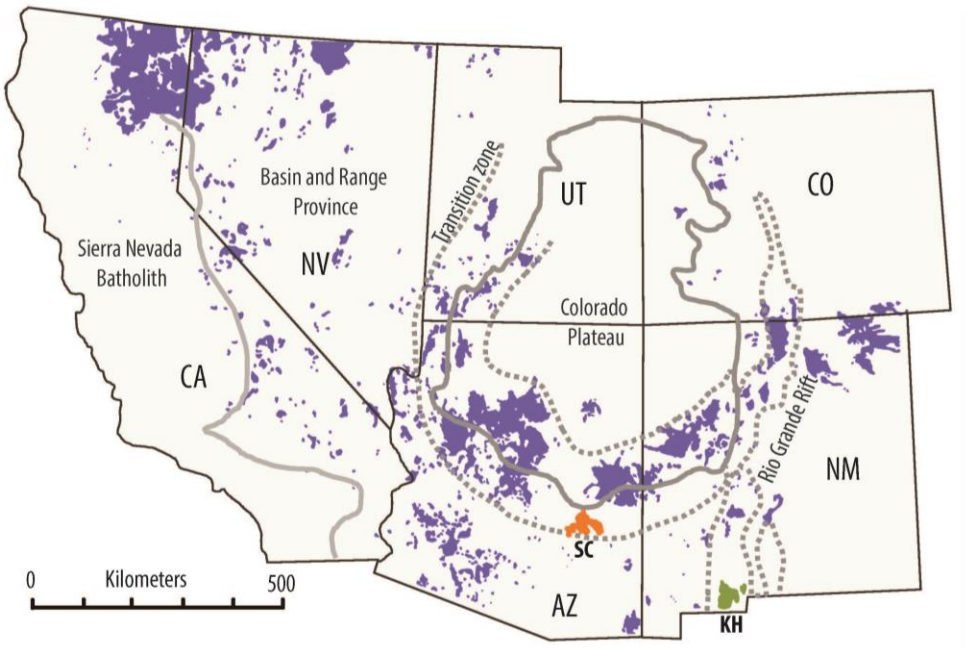

Fig. 1. Simplified sketch map of the southwestern United States showing the distribution of Cenozoic basaltic and basaltic andesite rocks, within the context of major physiographic provinces of the region, modified after Kempton (1991). The locations of mantle xenoliths collected for this study are shown in orange – San Carlos, AZ – and green – Kilbourne Hole, NM.

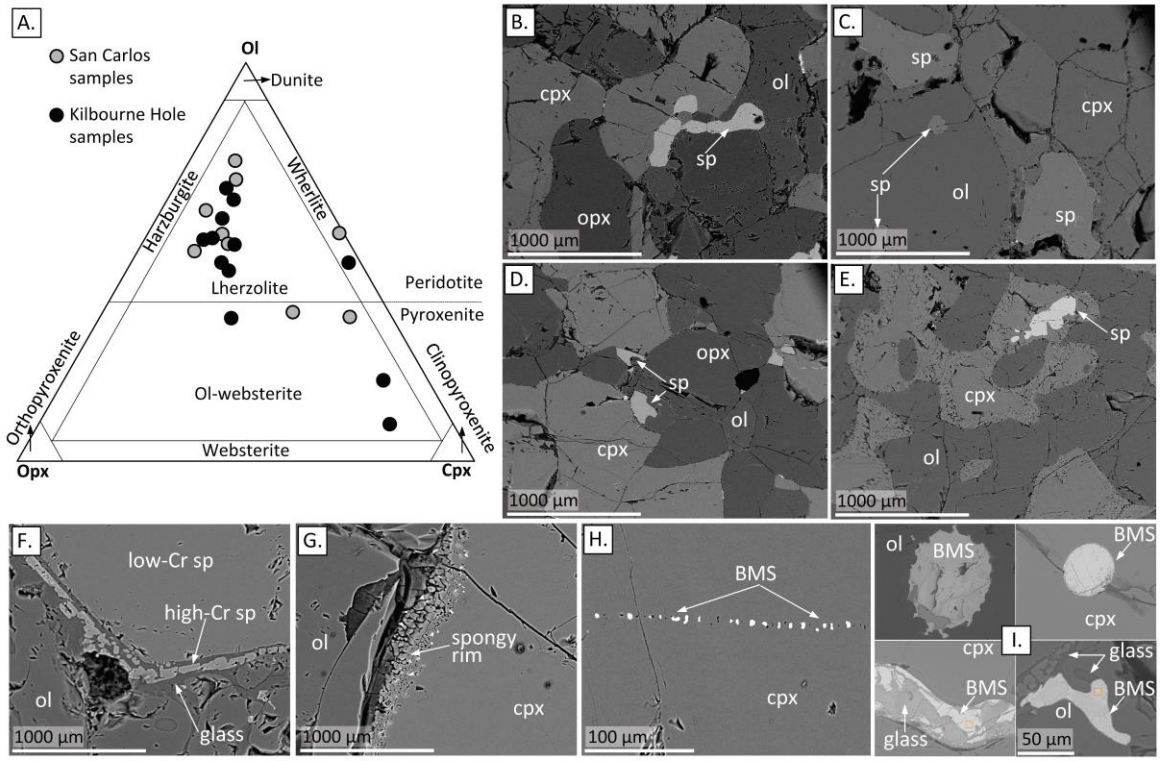

Fig. 2. A. Mineral modal composition for the investigated xenolith samples. B – I: Back-scattered electron photomicrographs of representative textures observed in the studied samples: B – protogranular (SC06); C – porphyroclastic (KH22); D – equigranular (SC11); E – poikilitic (SC09).

San Carlos xenoliths show a wide variation of textures, which we classified using the systematics of Mercier, Nicolas (1975). The predominant textural type is protogranular (SC02, SC03, SC04, SC05, SC06, SC13), with medium to coarse grained, dominantly equant crystals of olivine and orthopyroxene (1–5 mm) and much smaller clinopyroxenes and spinels. The grain boundaries tend to be curvilinear although, locally, polygonal aggregates of same mineral forming triple junctions were observed. Spinels occur mainly as interstitial, vermicular shaped grains, or rounded blebs enclosed in peripheral parts of orthopyroxenes. Rare polygonal spinel crystals have been detected. The samples display no evident mineral elongation, which could define any lineation or foliation to the rocks.

Porphyroclastic texture is present in one sample (SC10). The sample hosts large, elongated porphyroclasts of orthopyroxene (up to 8 mm) within a matrix of fine to medium grained, polygonal neoblasts of olivine and clinopyroxene (representing approximately 50% of the sample). The orthopyroxene porphyroclasts have irregular shapes with curved boundaries, and are slightly aligned, imprinting a weak foliation to the sample. Spinel occurs as a subordinate phase, with irregular grain shape, either fully enclosed or peripheral to olivine crystals. Several larger clinopyroxene crystals contain annealed cracks, forming trails of minute sulfide and fluid inclusions without any preferred orientation.

Two samples have mosaic equigranular textures (SC09 and SC11). They are characterized by fine-grained, equant crystals, with straight-lined grain boundaries, often converging at triple point junctions. Spinels mainly occur as small, disseminated grains, with curvilinear boundaries. Some spherical spinel inclusions were observed within olivine crystals. The equigranular samples show no textural anisotropy.

Poikilitic texture has been observed in the wehrlite sample (SC07). The sample is coarse grained (2–3 mm average), and it contains large poikilitic clinopyroxene crystals that enclose rounded grains of olivine. Spinels are scattered throughout the sample as small blebs fully enclosed in clinopyroxenes. Orthopyroxenes were absent in this sample. Interstitial glass is present, and it occurs as a discontinuous network of melt pockets surrounding the silicate minerals. Locally, tiny quench crystals of apatite and plagioclase were found in association with melt pockets. No other discrete metasomatic phases were identified, even though amphiboles (pargasite, kaersutite) and phlogopite have been reported previously at this location, especially in Group II xenoliths (Frey, Prinz, 1978).

Most samples lack any visible reaction products (pyrometamorphic textures) commonly developed through decompression-induced partial melting and melt infiltration during xenolith transport. Only three samples (SC04, SC07 and SC09) have clinopyroxenes with porous (spongy-textured) outer margin, indicative of an incipient partial melting reaction. The spongy border zones are thin (20–30 μm) and well delimited from the inner, homogeneous cores.

Sulfides are scarce (average 3 grains per polished section) or absent in San Carlos samples. They are small (20–40 μm) and occur mostly as isolated spheroidal droplets enclosed in clinopyroxenes. Some sulfide inclusions display irregular margins, with apophyses radiating from the rims, considered to be decrepitation features resulted during the entrainment of the xenoliths in the basaltic magma. Similar features in San Carlos xenoliths have been first described by Andersen *et al.* (1987). Linear or curved healed fractures in clinopyroxenes may have associated trails of minute sulfide and fluid inclusions. Interstitial sulfides have been also observed; they have either irregular, elongated shapes, and occur along curvilinear silicate grain boundaries or rounded blebs located at triple junctions, commonly in close association with glass pockets.

Kilbourne Hole samples examined for this study (n=11) are Cr-diopside bearing spinel lherzolites (n=8), spinel-bearing olivine websterites (n=2) and spinel wehrlite (n=1) (Fig. 2). All samples belong to Group I of Frey, Prinz (1978) and display predominantly protogranular and subordinately porphyroclastic – tabular equigranular textures, according to the texture classification of Mercier, Nicolas (1975).

Samples with protogranular texture (KH21, KH25, KH26, KH27, KH28, KH30, and KH31) have coarse olivine and orthopyroxene grain size (2–4 mm), with mostly curvilinear grain boundaries. Locally, olivine crystals form aggregates with polygonal boundaries. Clinopyroxenes are significantly smaller and occur in direct contact with larger orthopyroxene crystals. Spinels have amoeboid shapes, occurring commonly as interstitial blebs around orthpyroxene grains. Textural anisotropy or deformation features are absent in this sample group.

Samples with porphyroclastic transitioning into tabular equigranular texture (KH22, KH32, KH33, and KH35) have finer grain size (< 1mm) with few larger, elongated, porphyroclastic olivine and orthopyroxene crystals. Grain boundaries are straight-lined, commonly forming triple point jonctions. Clinopyroxenes form small, polygonal grains scattered in the samples. Spinels occur both as rounded to sub-rounded inclusions in olivine and as interstitial, xenomorphic shaped grains. Abundant intergranular spinels display the characteristic holly-leaf shape, but some well-developed, subhedral crystals are also present. The samples show weak lineation, characterized mainly by the alignment of elongated spinel grains.

With the exception of sample KH22, Kilbourne Hole samples studied here show no evidence of reaction or alteration of their primary mineralogy during transport. Interstitial spinel grains in sample KH22 show thin (approximately 20 μm) reaction coronas comprising small grains of partially interconnected secondary, high-Cr spinels surrounded by glass. Spinels display sharp boundaries between the core and the rim, and their cores show no evident zoning pattern.

No hydrous mineral phases were identified in the Kilbourne Hole samples used in this study. Sulfides are a very minor phase, with maximum five grains per polished section. Some samples are completely devoid of sulfides. Where present, sulfides are small (< 50 μm across), round blebs fully enclosed within silicate phases (mainly clinopyroxenes) or discrete, interstitial grains located at grain boundaries, commonly in association with melt pockets.

3. ANALYTICAL METHODS

3.1. ELECTRON-PROBE MICRO ANALYSIS

Major element, along with selected trace element compositions for the major, rock-forming silicates (olivines, clinopyroxenes, and orthopyroxenes) and spinels were analyzed in polished thick sections of approximately 1 mm thickness. We used a Cameca SX-100 electron-probe microanalyzer at the Lunar and Planetary Laboratory, University of Arizona. Five spectrometers were employed using the crystal arrangements TAP, LPET, LPET, TAP, LLIF. The instrument was calibrated using well-characterized natural and synthetic standards. During each analysis, major elements (Na Kα, Mg Kα, Al Kα, Si Kα, K Kα, Ca Kα, Mn Kα, Fe Kα, Ti Kα, and Ba Lα for silicate minerals; plus Cr Kα for oxides) were measured at 20 kV accelerating voltage and 20 nA beam current, counting for 10 seconds on peak. Beam conditions were then changed to high-current (299 nA, at 20 kV accelerating voltage) and longer counting time for the measurement of selected trace elements (F Kα, P Kα, S Kα, Cl Kα, Cr Kα, Sc Kα, V Kα, Ni Kα, Co Kα, Zn Lα, Y Lα, Ga Lα, Zr Lα, Sr Lα, Sn Lα, As Lα, Pb Mα). Representative mineral compositions are reported in Appendix 1 (available at https://osf.io/rkv38). Further details regarding the analytical routines used in this study are available at https://www.rockptx.com/wp-content/uploads/ 2017/02/microprobe-analytical-routines-2016.pdf.

3.2. LASER ABLATION INDUCTIVELY COUPLED PLASMA MASS SPECTROMETRY

Major and trace element concentrations in olivines, clinopyroxenes, orthopyroxenes, and spinels were obtained *in situ* by laser ablation inductively coupled plasma mass spectrometry (LA-ICP-MS)

on the same thick sections used for electron probing. The analyses were conducted on an Agilent 7500a ICP-MS instrument, coupled to a GeoLas 2005, 193 nm wavelength laser ablation system, at the State Key Laboratory of Geological Processes and Mineral Resources, China University of Geosciences. Laser sampling was performed in He carrier gas, single spot ablation style, with a laser beam diameter of 40 μm. Data acquisition time for each analysis was set to 50 seconds on sample, followed by approximately 20 seconds of background acquisition. Well-characterized reference glasses of natural and synthetic compositions such as NIST: SRM 610 (Pearce *et al*., 1997), USGS: BCR-2G, BHVO-2G, BIR-1G, GSD-1G, GSE-1G (Jochum *et al.*, 2005) and MPI-DING: ATHO-G, ML3B-G, T1-G (Jochum *et al*., 2006) were used after every 8 sample analyses. An in-house software (ICPMSDataCal) was used to perform time-dependent drift of sensitivity and mass discrimination correction and quantitative data calibration. More detailed operating conditions, data calibration strategy and software, as well as method uncertainties are found in Liu *et al.* (2008). Analyses are reported in Appendix 2 (available at https://osf.io/rkv38).

4. RESULTS

4.1. MANTLE MINERAL CHEMISTRY: MAJOR AND TRACE ELEMENTS

Olivine, clinopyroxene, orthopyroxene and spinel grains were analyzed in detail, with 1–4 grains per phase, cores and rims, for each sample (EMPA and LA-ICP-MS combined). Full mineral datasets are available in Appendix 1 and 2 (available at https://osf.io/rkv38). Minerals in the studied mantle xenoliths are generally chemically homogeneous, showing no considerable inter- and intra-grain compositional variation.

4.1.1. Olivine

In San Carlos (SC) samples, olivine crystals have forsterite content (Fo; = 100 x Mg/ (Mg + Fe), normalized cation ratios) ranging between 87.8 and 89.7 for lherzolites and slightly more elevated Fo contents for the olivine websterite samples (88.5–90.9) (Fig. 3), with comparable and limited ranging NiO (0.35–0.42 wt.%) and MnO contents (0.10 – 0.18 wt.%). Calcium content shows more variability (0.034–0.127 wt.% CaO), from sample to sample, but also from core to rim. Many olivines, especially in the websterite sample group, have more elevated Ca contents towards the rims (up to 60% increase of Ca at the rims of the grains). The olivines in the wehrlite sample have the lowest Fo content observed (70.7), lower NiO (0.21 wt.%), and higher MnO (0.32–0.37 wt.%). Its calcium content from core to rim is 0.027–0.130 wt.% oxide, which is the most significant rim enrichment for Ca in the San Carlos samples.

Olivines belonging to Kilbourne Hole (KH) lherzolite and websterite samples are largely similar in their major element content. The lherzolite olivine Fo content ranges between 87.6 and 89.6, and NiO between 0.37 and 0.42 wt.%, while the websterite olivines have 87.7–89.4% Fo and 0.36 –0.40 wt.% NiO compositions (Fig. 3). Their Mn and Ca content overlaps as well, although the lower and the higher ends of the range are characteristic to lherzolite (0.09–0.16 wt.% MnO; 0.025 –0.084 wt.% CaO) and websterite samples (0.12–0.18 wt.% MnO; 0.035–0.093 wt.% CaO), respectively. Few olivine crystals in the KH sample set show Ca compositional variation, including normal (where Ca content increases at rims) and reverse (where Ca contents decreases at rims) core-rim zoning patterns. However, Ca variation in KH samples is less pronounced than in the SC samples investigated here (up to 25% Ca increase in KH26-lherzolite, KH31-websterite, KH28-wehrlite). The KH wehrlite sample has olivines with low Fo (81.5), and NiO (0.26 wt.%), and high MnO (0.21 wt.%). Calcium concentration is also higher than other KH samples (0.10–0.14 wt.%), but with much attenuated core-to-rim variation compared the SC wehrlite.

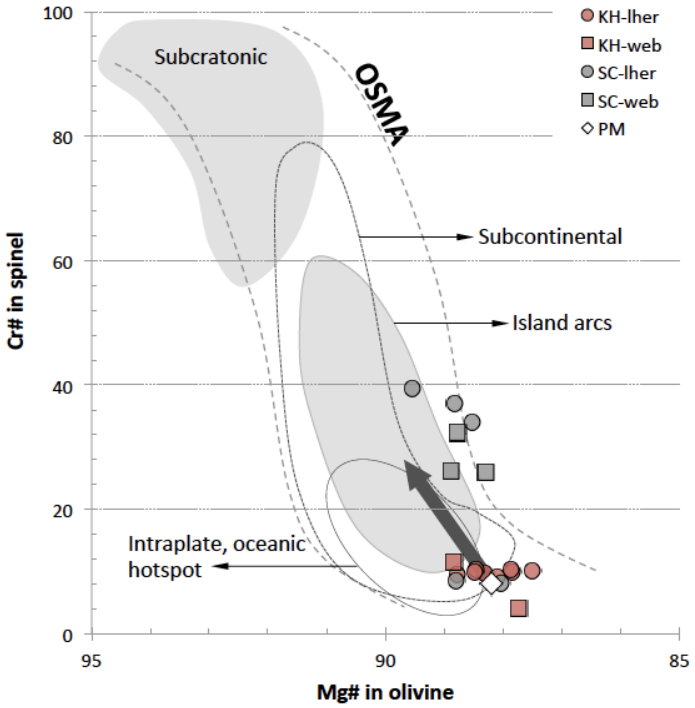

Fig. 3. Plot of spinel Cr-number vs. olivine Mg-number for peridotites (circles) and pyroxenites (squares) from Kilbourne Hole (KH, red symbols) and San Carlos (SC, grey symbols), within the olivine-spinel mantle array (OSMA), of Arai (1994). Domains for various tectonic settings (Arai, 1994) are shown for comparison. The melt depletion trend, marked by an arrow, is projected from the Primitive Mantle (PM) composition of McDonough, Sun (1995). Cr# = 100 x Cr / (Cr + Al); Mg# = 100 x Mg / (Mg + Fe_{tot}), normalized cation ratios; Fe_{tot} = total iron as ferrous. Wehrlite samples were not plotted owing to their low (< 85) Mg#. Lher– lherzolite; web – websterite.

4.1.2. Clinopyroxene

San Carlos lherzolite samples have clinopyroxenes with an end-member composition of $Wo_{42-45}En_{49-52}Fs_{4-6}$ and Mg# ranging between 89.34 and 91.98. They are mostly homogeneous with respect to Ti, Al and Na concentrations. Their TiO_2 content ranges between 0.11 and 0.54 wt.%, Al_2O_3 between 3.27 and 7.35 wt.%, and Na_2O between 1.06 and 2.24 wt.%. Chromium displays the largest amplitude of variation between SC lherzolites, with Cr# falling mainly into two distinct compositional groups: a more fertile group with Cr# values of 5.74–7.58 (SC04 and SC05), and a more refractory group with Cr# of 12.97–22.63 (SC02, SC03, SC06, SC13). The SC pyroxenites have a clinopyroxene composition of $Wo_{21-46}En_{49-70}Fs_{4-8}$, with Mg# between 88.79 and 91.86, more elevated Cr, Al and Ti contents (Cr#: 8.70–16.97; 4.38–13.55 wt.% Al_2O_3; and 0.23–2.40 wt.% TiO_2). Sodium is low (0.60–1.32 wt.% Na_2O) with the exception of sample SC09 where Na_2O is slightly higher (2.04–3.51 wt.%) and variable from grain to grain, without any core-to-rim heterogeneity. The wehrlite clinopyroxenes are Ti-augites characterized by an end-member composition of $Wo_{37-47}En_{42-48}Fs_{11-14}$, and by Mg# and Cr# as low as 77.5 and 1.12, respectively. Weak inter-grain compositional variation is observed, with TiO_2 content of 0.71–1.21 wt.%; 5.80 –8.20 wt.% for Al_2O_3; and 1.05–1.19 wt.% for Na_2O.

All clinopyroxenes in Kilbourne Hole mantle xenoliths are Cr-diopsides having relatively similar end-member compositions of $Wo_{43-46}En_{48-50}Fs_{5-6}$ for lherzolites, $Wo_{44-47}En_{48-50}Fs_{5-6}$ for olivine websterites, and $Wo_{42-44}En_{44-48}Fs_{9-12}$ for the wehrlite sample. KH lherzolites tend to be less refractory than the SC equivalents, with slightly lower Mg# (88.7–90.57), NaO_2 (1.56–1.98 wt.%), and Cr# (4.02–8.33), but richer in TiO_2 content (0.23–0.63 wt.%). The compositions of clinopyroxenes in the

websterite samples lie within the range of those analyzed in lherzolite with respect to their end-member configuration and Mg# (89.28–90.52). They are characterized also by lower Na_2O (0.41–1.93 wt.%), and moderate enrichment in Al and Ti contents (5.79–8.66 wt.% Al_2O_3, 0.44–0.80 wt.% TiO_2). Chromium shows wider variation from sample to sample, with Cr# as low as 1.10–3.24 for sample KH31, and 8.73–8.94 for KH35. In contrast, the wehrlite sample has clinopyroxenes with remarkably low Mg#, between 78.35 and 83.59, and Cr#, between 0.16 and 6.21. On the other hand, clinopyroxenes are richer in Ti and Al (0.76–1.60 wt.% TiO_2, and 7.50–9.25 wt.% Al_2O_3). In this sample, sodium has a limited range of variation (1.32–1.42 wt.% oxide).

4.1.3. Orthopyroxene

Orthopyroxenes in San Carlos samples are enstatite with similar end-member compositions ($Wo_{1-2}En_{87-89}Fs_{9-10}$ in lherzolites, and $Wo_{1-2}En_{88-90}Fs_{9-11}$ in olivine websterites). No orthopyroxenes were identified in the SC wehrlite sample. Lherzolite orthopyroxenes have Mg# ranging between 88.9 and 90.5, Cr# between 4 and 15.5, and are relatively Al-rich (2.3–5.4 wt.% Al_2O_3), and Na and Ti poor (0.07–0.18 wt.% Na_2O, and 0.04–0.16 wt.% TiO_2). In comparison, orthopyroxenes belonging to olivine websterite samples are slightly more magnesian (Mg# 89–91.2), and have a more limited Cr# range (6.19–12.8) than the lherzolite-hosted orthopyroxenes, but otherwise, their major element compositions overlap entirely. Most grains show moderate Al, Cr, Ca and Ti zonation, with higher contents in cores than in rims.

Orthopyroxenes in Kilbourne Hole xenoliths are enstatite with end-member compositions of $Wo_{1-2}En_{88-89}Fs_{10-11}$ for lherzolites, and $Wo_{1-2}En_{87-88}Fs_{10-11}$ in olivine websterites, and with slightly higher ferrosilite component for the wehrlite sample ($Wo_2En_{84}Fs_{14}$). Lherzolite- and websterite-hosted orthopyroxenes are characterized by a narrow range of Mg# (from 88.5 to 90.2) and Cr# (between 2.8 and 6.4), and by moderate contents of Na and Ti (0.08–0.14 wt.% Na_2O; 0.05–0.16 wt.% TiO_2). Aluminum content ranges between 3.7 and 5.2 wt.% Al_2O_3 and shows no significant zonation. Orthopyroxenes in the wehrlite sample have Mg# of 85.5, Cr# of 5.3, are, in average more aluminous (5.3–5.4 wt.% Al_2O_3), Ti and Na rich (0.17 wt.% TiO_2, 0.14 wt.% Na_2O). The analyzed orthopyroxene grains in the wehrlite sample preserve a weak variation in major elements, expressed by core-to-rim enrichment in Ca, Ti and Al, compensated by depletion in Cr and Mg.

4.1.4. Spinel

Spinels from San Carlos lherzolites and websterites show a similar and broad compositional range, characterized mainly by extensive substitution along the spinel ($MgAl_2O_4$) – magnesiochromite ($MgCr_2O_4$) solid solution ($Cr_{0.16-0.78}Al_{1.15-1.83}$; atoms per formula unit – a.p.f.u.), and rather limited substitution along the spinel – hercynite ($FeAl_2O_4$) end-member composition series ($Mg_{0.70-0.81}Fe^{2+}_{0.19-0.30}$). As a result, lherzolite- and websterite-hosted spinels display a wide range of Cr# (8.2–40.3) and consistently low values for Mg# (70–81). They also contain trace amounts of Fe^{3+} (up to 0.10 a.p.f.u., calculated), and minor amounts of Ti and Mn (0.11–0.34 wt.% TiO_2, and 0.08 –0.19 wt.% MnO). In contrast, spinels belonging to the wehrlite sample are rich in the hercynite component ($Mg_{0.50-0.52}Fe^{2+}_{0.48-0.50}$), and also contain higher amounts of Fe^{3+} (0.11 a.p.f.u.), TiO_2 (0.42 wt.%), and MnO (0.19–0.22 wt.%). The wehrlite-hosted spinels are significantly less chromian (Cr# < 14) and less magnesian (Mg# < 52) than those in other SC samples studied here.

Kilbourne Hole lherzolites and websterites contain spinels that are highly magnesian (Mg# ranging between 78.6 and 92.1, where the lower values represent mostly the lherzolites, while the higher values, the websterites), and low chromium contents (Cr# ranging between 0.76 and 11.5). Their end-member composition is dominated by spinel and show limited substitution along the spinel –

magnesiochromite and spinel – hercynite solid solution series ($Cr_{0.02-0.21}Al_{1.64-1.94}$; $Mg_{0.79-0.92}Fe^{2+}_{0.08-0.21}$). In addition to these major elements, KH lherzolite- and websterite-hosted spinels also contain small amounts of Fe^{3+} (up to 0.16 a.p.f.u.), Ti (0.02–0.13 wt.% oxide), and Mn (0.05 –0.13 wt.% oxide). The KH wehrlite contains spinels that belong to the spinel – hercynite solid solution series ($Mg_{0.67-0.76}Fe^{2+}_{0.24-0.34}$), with relatively high amounts of Ti (0.48–0.66 wt.% oxide), and Fe^{3+} (0.08–0.2 a.p.f.u., calculated). The KH wehrlite spinels are also characterized by extremely low Mg# (66.7–75.8), and Cr# (0.26–2.79).

4.2. TRACE ELEMENT COMPOSITIONS OF CLINOPYROXENES

Trace element abundances in clinopyroxenes from San Carlos xenoliths show significant light rare earth elements (LREEs) scattering, and nearly flat or smoothly descending slope for middle and heavy rare earth elements (MREEs and HREEs, respectively) (Fig. 4.A). Most clinopyroxenes in the San Carlos lherzolites display relatively flat MREE-HREE patterns, with wide range of CI chondrite-normalized MREE and HREE concentrations, $(MREE)_{CI}$ = 5.8–44.1; $(HREE)_{CI}$ = 1.74 –24.2; $(Yb)_{CI}$ = 1.74–14.8, and various degrees of LREE depletion, with $(Ce/Yb)_{CI}$ between 0.12 and 0.98. As exceptions, lherzolites SC06 and SC02 contain clinopyroxenes with marked upward convex REE patterns with apexes at cerium values, which show significant relative LREE enrichments, $(Ce/Yb)_{CI}$ = 4.56–3.05. Websterite-hosted clinopyroxenes at San Carlos have LREE abundances that vary from relatively depleted, $(Ce/Yb)_{CI}$ = 0.64–0.99 (SC10 and SC11), to highly enriched $(Ce/Yb)_{CI}$ = 5.6 (SC09); while their MREE and HREE concentrations are confined to a narrower range than in SC lherzolites, $(MREE)_{CI}$ = 4.66–31.5; $(HREE)_{CI}$ = 2.45–12.8; $(Yb)_{CI}$ = 2.45–12.3. The wehrlite sample contains clinopyroxenes with LREE-enriched profile $(Ce/Yb)_{CI}$ = 4.5–5.1, and ample core to rim LREE and MREE enrichments (La_{core} = 4.6 ppm; La_{rim} = 5.4 ppm; Ce_{core} = 12.1 ppm; Ce_{rim} = 18.3 ppm; Nd_{core} = 6.5 ppm; Nd_{rim} = 11.4 ppm; Sm_{core} = 1.6 ppm; Sm_{rim} = 3.5 ppm; Eu_{core} = 0.8 ppm; Eu_{rim} = 1.3 ppm;).

Primitive mantle-normalized extended trace element patterns of clinopyroxenes in the majority of San Carlos samples (Fig. 4.B) are characterized by overall enrichments in the highly incompatible elements (Th, U, LREE), with marked negative Nb anomalies relative to the LREE, and depletions of Sr, Ti, Zr and Hf relative to elements with similar incompatibilities; Sr/Sr* = 0.42–0.88; Ti/Ti* = 0.16–0.78; Zr/Zr* = 0.24 – 0.68; and Hf/Hf* = 0.1–0.85, (where: Sr* = (Pr + Nd)/2; Ti* = (Eu + Gd)/2; and Zr* and Hf* = (Nd + Sm)/2). Few lherzolite-hosted clinopyroxenes show positive deviations for Hf/Hf* = 1–1.3, in the core of SC05 and in the rim of SC04, and Sr/Sr* = 1.03–1.04, in sample SC02, core and rim, and in the core of SC03.

Clinopyroxene REE patterns from Kilbourne Hole xenoliths (Fig. 4.C) are similar to our San Carlos patterns, with respect to LREE scattering, but display a smoother slope and narrower range of values for the MREEs and HREEs. All analyzed Kilbourne Hole lherzolites contain clinopyroxenes with pronounced LREE depletions, $(Ce/Yb)_{CI}$ = 0.05–0.52, and narrow range for MREE and HREE concentrations, $(MREE)_{CI}$ = 7.2–14.4; $(HREE)_{CI}$ = 6.5–15.1; $(Yb)_{CI}$ = 8–13. Core-rim variation is generally not remarkable, except for samples KH21 and KH22, which display more significant rim enrichments in the most incompatible LREEs (La_{core} = 0.02 ppm; La_{rim} = 0.12 ppm in lherzolite KH21, and La_{core} = 0.42 ppm; La_{rim} = 1.2 ppm; Ce_{core} = 1.71 ppm; Ce_{rim} = 2.66 ppm in lherzolite KH22). The two websterite samples in the Kilbourne Hole sample suite have contrasting trace element patterns. Websterite KH35 has a smoothly ascending LREE slope, peaking at Eu values, with lightly depleted LREE, $(Ce/Yb)_{CI}$ = 0.7, and relatively flat MREE and HREE patterns, with values clustering closely around 10 x CI chondrite, resembling the patterns observed in KH lherzolites. In contrast, websterite KH31 has LREE-enriched clinopyroxenes with pronounced convex upward REE patterns with apex at neodymium ($(Nd)_{CI}$ = 41), and steadily descending slope in the MREE and HREE ranges ($(MREE)_{CI}$ = 20–35; $(HREE)_{CI}$ = 8.3–20.8), very similar to the wehrlite sample KH28. Websterite KH31 has a

LREE/HREE ratio of $(Ce/Yb)_{CI}$ = 3.2, while the wehrlite KH28 has a slightly lower LREE/HREE value of $(Ce/Yb)_{CI}$ = 2.3.

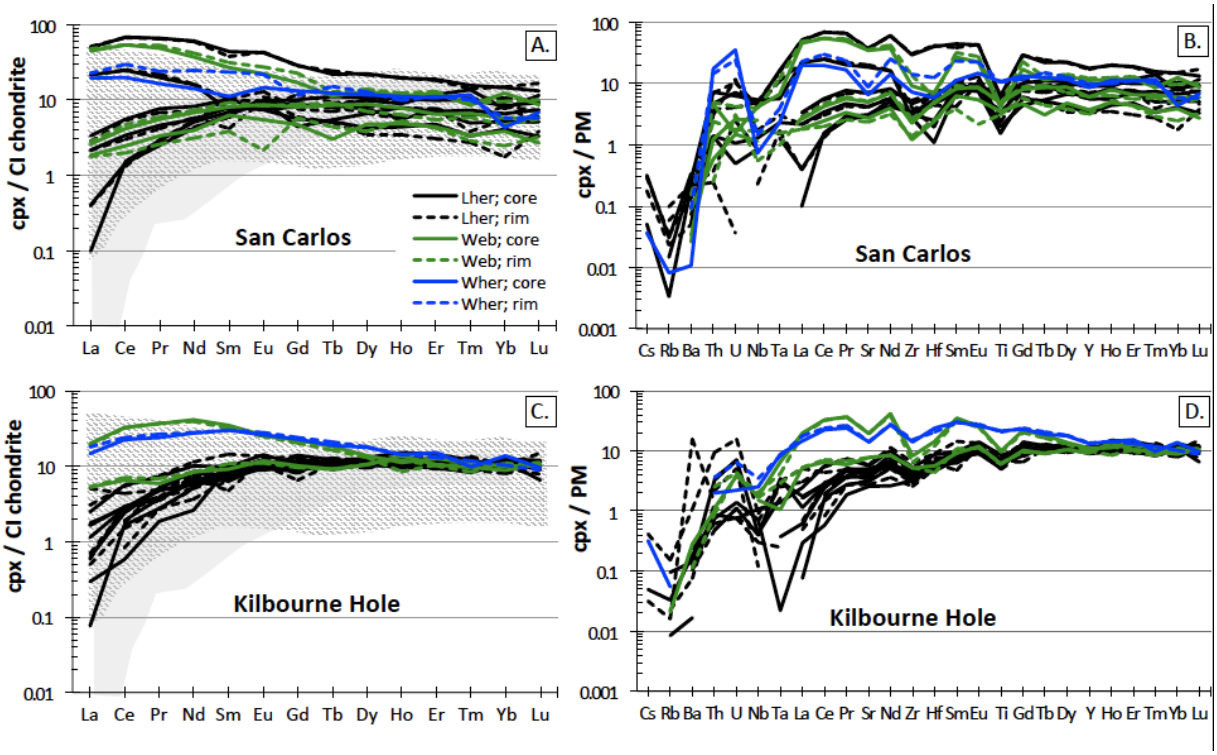

Fig. 4. CI chondrite-normalized rare earth element (REE) (panels A and C) and Primitive mantle (PM)-normalized extended trace element abundances (panels B and D) of clinopyroxenes (cpx) from San Carlos and Kilbourne Hole mantle xenoliths. Clinopyroxenes and whole-rock REE compositions from various localities of mantle xenoliths along the Laramide corridor (diagonal pattern field) (Geronimo, AZ: Menzies *et al*., 1985; Wikieup, AZ: McGuire, Mukasa, 1997; Dish Hill and Cima, CA: Luffi *et al*., 2009; Kilbourne Hole, NM: Harvey *et al*., 2012; Cemetery Ridge, AZ: Haxel *et al*., 2015; Crystal Knob, CA: Quinn *et al*., 2018), as well as for abyssal peridotites (solid grey field) from Johnson *et al*. (1990) are shown for comparison. Normalizing values are from McDonough and Sun (1995). Solid lines represent mineral core values, whereas dashed lines represent mineral rim values. Lher – lherzolite; web – websterite; wher – wehrlite. The legend in panel A applies to the entire figure.

Primitive mantle-normalized extended trace element patterns of clinopyroxenes in the Kilbourne Hole samples (Fig. 4.D) are defined by generalized depletion in large ion lithophile elements (LILEs) with the exception of a strong rim-enrichment in Ba, observed in lherzolite KH25, and by relative enrichments in the more incompatible high strength field elements (HFSEs), U and Th. Other, more compatible HFSE, such as Zr, Hf and Ti show variable degrees of depletion compared to adjacent elements in the pattern: Zr/Zr* = 0.18–0.75; and Hf/Hf* = 0.34–0.99; and Ti/Ti* = 0.42–0.88, where the lower end of the spectrum characterizes the websterite-hosted clinopyroxenes, while the higher end of the spectrum characterizes the lherzolite and wehrlite-hosted clinopyroxenes. Strontium content in KH lherzolites is limited to 18–42 ppm, and shows moderate negative anomalies Sr/Sr* = 0.57–0.93, and even small positive anomalies (Sr/Sr* = 1– 1.1) in sample KH30 and in the core of KH32. In wehrlite and websterite samples, Sr is distinctly enriched (56–142 ppm) but, due to comparable enrichments in similarly compatible elements, Sr/Sr* ratios remain within the range of KH lherzolite samples.

4.3. THERMOBAROMETRY

Thermometry was performed on mineral cores and rims using Brey, Kohler (1990) as well as the more recent calibration of Putirka (2008) (Fig. 5). Fig. 5 shows that there is very good agreement between the two calibrations and hardly any differences between cores and rims of rock forming minerals between the various lithologies. The temperature range is between 1000–1100 ^{0}C, which is clearly in the realm of lithospheric mantle temperatures, although they represent a hot lithospheric mantle. These values are fully consistent with determinations made previously by Galer, O'Nions (1989). Pressures of equilibration were calculated using Putirka (2008) and indicate depth ranges between 0.9–1.5 GPa, with the greater depths in that range characterizing the Kilbourne Hole xenoliths. This is consistent with the slightly deeper Moho know independently at that location (38 km) versus San Carlos where the Moho is at around 33 km. Overall our pressure-temperature calculations are consistent with the high heat flow values reported from Kilbourne Hole region (95 mW/m^2). Clearly, these xenoliths at both localities span the shallowest range of mantle (lithosphere) immediately below their respective Moho discontinuities but not deeper than ~ 50 km.

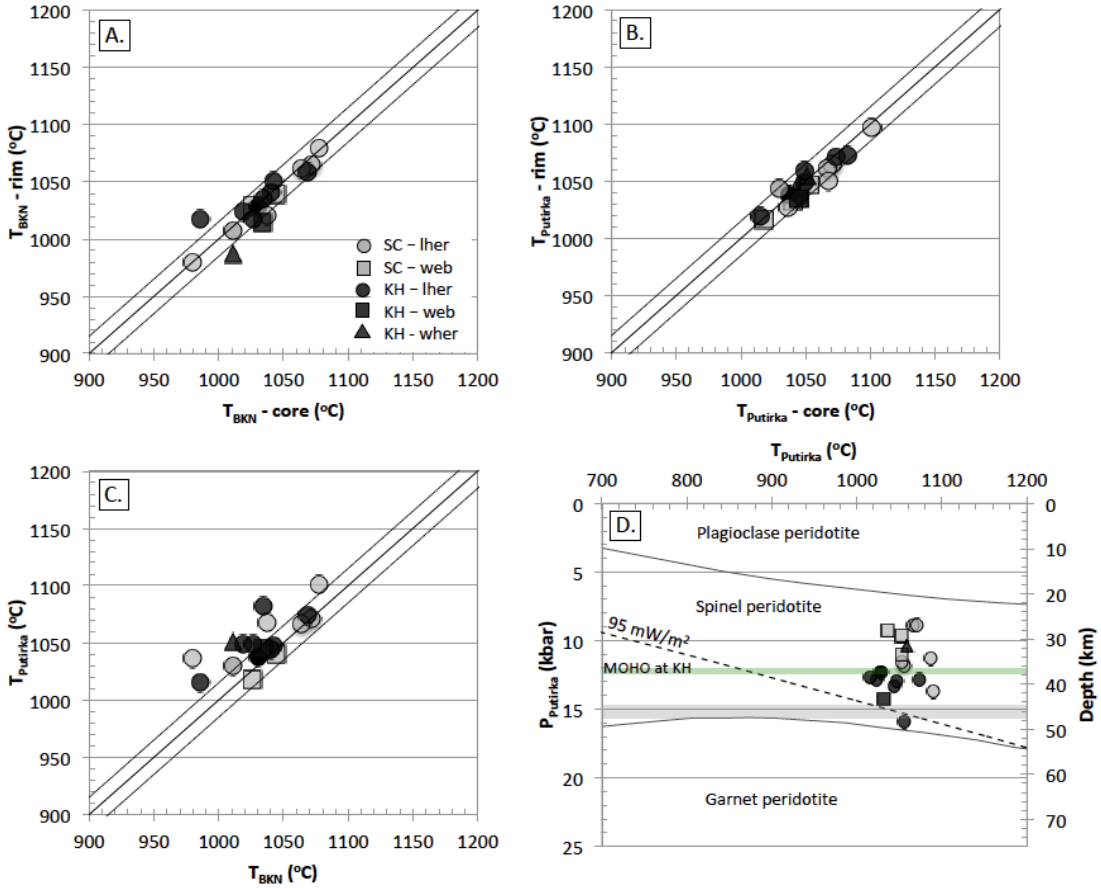

Fig. 5. Geothermobarometry on San Carlos (grey symbols) and Kilbourne Hole (black symbols) xenoliths: A. Correlation of core and rim temperatures calculated using major element-based two-pyroxene geothermometer of Brey, Köhler (1990), (T_{BKN}). Dashed lines represent 15^{0}C deviations from the 1:1 correlation line. B. Correlation of core and rim temperatures calculated using major element-based two-pyroxene geothermometer of Putirka (2008), ($T_{Putirka}$); C. Correlation of calculated core temperatures between the two geothermometers used: T_{BKN} and $T_{Putirka}$; D. P-T diagram, using calculated core temperatures ($T_{Putirka}$) and pressures ($P_{Putirka}$). Four-phase peridotite stability fields are from Gasparik (1984).

4.4. DEPLETION OF PERIDOTITES

Peridotites studies here have various degree of depletion based on modal mineralogy. However, most of them are lherzolites and do not show extreme depletions as seen in the suboceanic mantle (abyssal peridotites, etc.). One way of quantifying the amount of depletion is to use Y and Yb in clinopyroxenes from peridotites, in order to determine how depleted these peridotites are relative to a chondritic mantle (in %). This would broadly correspond to the percentage of melt lost from a chondritic-like mantle. Results of this simple forward model are shown in Fig. 6 for both San Carlos and Kilbourne Hole and show that the majority San Carlos and all of Kilbourne Hole peridotites display small (<5%) amounts of depletion, with a few outliers at San Carlos near the 10% depletion mark. These results as well as the overall trace elemental patterns in spiderdiagrams (Fig. 4) together argue against an oceanic mantle origin for these peridotites on melt depletion arguments alone. Radiogenic isotopes (Sr, Nd, Pb) (Galer, O'Nions, 1989) are more ambiguous at least for San Carlos, as they can be assigned to the MORB mantle field.

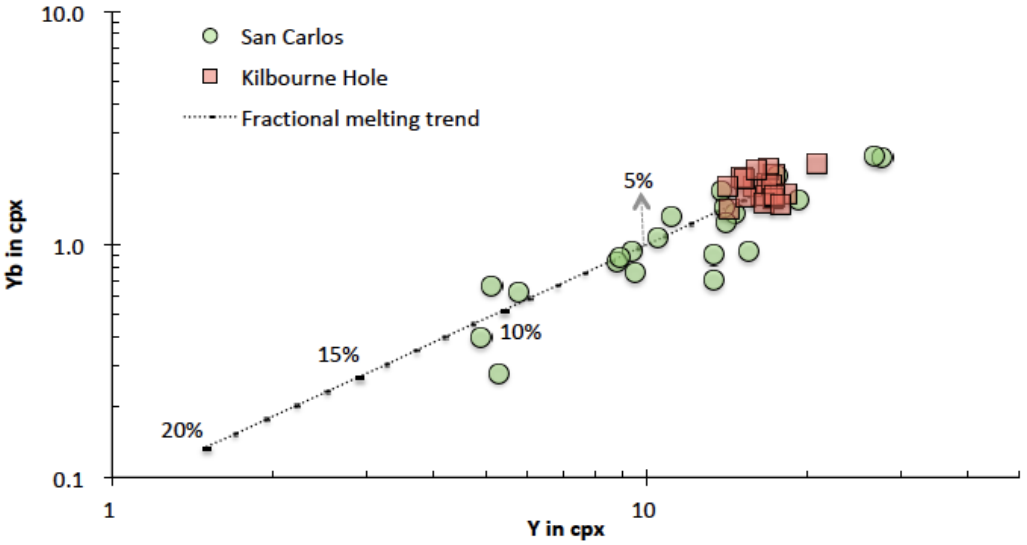

Fig. 6. Partial melting trends from Y and Yb in clinopyroxenes, following a generic model of fractional melting of a primitive chondritic mantle. Y_{PM}= 3.34 ppm; Yb_{PM}= 0.346 ppm from McDonough, Sun (1995).

5. INTERPRETATIONS

The results above have some important implications for the origin and age of the continental mantle lithosphere currently underlying the American Southwest at 30–50 km. We summarize them below:

a. The lack of any diffusional gradients from core to rim (cooling paths) suggest that temperatures are recent; in other words, the heating of the lithospheric mantle recorded by the xenoliths took place relatively recently, possibly during continental extension in the Quaternary at both locations;
b. The same argument applies to metasomatism, which is probably also recent, and related to the last Cordilleran orogenic cycle. It is unlikely that pyroxenite veins emplaced in a previous Wilson cycle would show such uniform temperatures from core to rim;

c. The mild depletion displayed by peridotites from both locations in both Mg# as well as trace elemental patterns is inconsistent with a Farallon (accreted oceanic slab) origin; instead the mantle lithosphere at both locations is interpreted to be native North American;
d. Key markers such as Cr# in spinels and Mg# in olivines are also inconsistent with a cratonic origin for the shallow mantle beneath the American Southwest; it is either a modified (re-fertilized) cratonic mantle or more likely one formed as the root of the Mid-Proterozoic terranes od the SW U.S.A and modified by Cordilleran-related metasomatism during the Cenozoic.

Acknowledgments. M.N.D. acknowledges support from the Romanian Executive Agency for Higher Education, Research, Development and Innovation Funding project PN-III-P4-ID-PCCF-2016-0014. Dr. Ken Domanik is thanked for his expert assistance in the Michael Drake Electron Microprobe Facility at Arizona. Dr. Wu Dan and Prof. Yongsheng Liu are thanked for assistance with data acquisition on the laser ablation ICP-MS at China University of Geosciences in Wuhan, China. Data are available as two Supplementary Excel files with multiple sheets on the open science data platform OSF at https://osf.io/rkv38. This contribution has the following document identifier available through osf.io: DOI 10.17605/OSF.IO/RKV38.

REFERENCES

Andersen, T., Griffin, W.L., O'Reilly, S.Y., 1987. *Primary sulphide melt inclusions in mantle-derived megacrysts and pyroxenites.* Lithos, *20*(4), pp. 279–294.

Arai, S., 1994. *Characterization of spinel peridotites by olivine-spinel compositional relationships: review and interpretation*. Chemical geology, *113*(3–4), pp. 191–204.

Brey, G.P., Köhler, T., 1990. *Geothermobarometry in four-phase lherzolites II. New thermobarometers, and practical assessment of existing thermobarometers*. Journal of Petrology, *31*(6), pp. 1353–1378.

Dromgoole, E.L., Pasteris, J.D., 1987. *Interpretation of the sulfide assemblages in a suite of xenoliths*. Mantle Metasomatism and Alkaline Magmatism, *215*, p. 25.

Frey, F.A., Prinz, M., 1978. *Ultramafic inclusions from San Carlos, Arizona: petrologic and geochemical data bearing on their petrogenesis*. Earth and Planetary Science Letters, *38*(1), pp. 129–176.

Galer, S.J.G., O'nions, R.K., 1989. *Chemical and isotopic studies of ultramafic inclusions from the San Carlos Volcanic Field, Arizona: a bearing on their petrogenesis*. Journal of Petrology, *30*(4), pp. 1033–1064.

Gasparik, T., 1984. *Experimental study of subsolidus phase relations and mixing properties of pyroxene in the system CaO-Al2O3-SiO2*. Geochimica et Cosmochimica Acta, *48*(12), pp. 2537–2545.

Harvey, J., Yoshikawa, M., Hammond, S.J., Burton, K.W., 2012. *Deciphering the trace element characteristics in Kilbourne Hole peridotite xenoliths: melt–rock interaction and metasomatism beneath the Rio Grande Rift, SW USA*. Journal of Petrology, *53*(8), pp. 1709–1742.

Haxel, G.B., Jacobson, C.E., Wittke, J.H., 2015. *Mantle peridotite in newly discovered far-inland subduction complex, southwest Arizona: Initial report*. International Geology Review, *57*(5–8), pp. 871–892.

Jochum, K.P., Stoll, B., Herwig, K., Willbold, M., Hofmann, A.W., Amini, M., Aarburg, S., Abouchami, W., Hellebrand, E., Mocek, B., Raczek, I., 2006. *MPI-DING reference glasses for in situ microanalysis: New reference values for element concentrations and isotope ratios.* Geochemistry, Geophysics, Geosystems, *7*(2).

Jochum, K.P., Willbold, M., Raczek, I., Stoll, B., Herwig, K., 2005. *Chemical Characterisation of the USGS Reference Glasses GSA-1G, GSC-1G, GSD-1G, GSE-1G, BCR-2G, BHVO-2G and BIR-1G Using EPMA, ID-TIMS, ID-ICP-MS and LA-ICP-MS*. Geostandards and Geoanalytical Research, *29*(3), pp. 285–302.

Johnson, K.T., Dick, H.J., Shimizu, N., 1990. *Melting in the oceanic upper mantle: an ion microprobe study of diopsides in abyssal peridotites*. Journal of Geophysical Research: Solid Earth, 95(B3), pp. 2661–2678.

Kempton, P.D., Fitton, J.G., Hawkesworth, C.J., Ormerod, D.S., 1991. *Isotopic and trace element constraints on the composition and evolution of the lithosphere beneath the southwestern United States.* Journal of Geophysical Research: Solid Earth, 96(B8), pp. 13713–13735.

Liu, Y., Hu, Z., Gao, S., Günther, D., Xu, J., Gao, C., Chen, H., 2008. *In situ analysis of major and trace elements of anhydrous minerals by LA-ICP-MS without applying an internal standard*. Chemical Geology, 257(1–2), pp. 34–43.

Luffi, P., Saleeby, J.B., Lee, C.T.A., Ducea, M.N., 2009. *Lithospheric mantle duplex beneath the central Mojave Desert revealed by xenoliths from Dish Hill, California*. Journal of Geophysical Research: Solid Earth, 114(B03202).

McDonough, W.F., Sun, S.S., 1995. *The composition of the Earth.* Chemical geology, 120(3–4), pp. 223–253.

McGuire, A.V., Mukasa, S.B., 1997. *Magmatic modification of the uppermost mantle beneath the Basin and Range to Colorado Plateau Transition Zone; Evidence from xenoliths, Wikieup, Arizona*. Contributions to mineralogy and petrology, 128(1), pp. 52–65.

Menzies, M., Kempton, P., Dungan, M., 1985. *Interaction of continental lithosphere and asthenospheric melts below the Geronimo volcanic field, Arizona, USA*. Journal of Petrology, 26(3), pp. 663–693.

Pearce, N.J., Perkins, W.T., Westgate, J.A., Gorton, M.P., Jackson, S.E., Neal, C.R., Chenery, S.P., 1997. *A compilation of new and published major and trace element data for NIST SRM 610 and NIST SRM 612 glass reference materials*. Geostandards Newsletter, 21(1), pp. 115–144.

Putirka, K.D., 2008. *Thermometers and barometers for volcanic systems.* Reviews in mineralogy and geochemistry, 69(1), pp. 61–120.

Quinn, D.P., Saleeby, J., Ducea, M., Luffi, P., Asimow, P., 2018. *Late-Cretaceous construction of the mantle lithosphere beneath the central California coast revealed by Crystal Knob xenoliths*. Geochemistry, Geophysics, Geosystems, 19(9), p. 3302–3346.

Uchida, H., Lavina, B., Downs, R.T., Chesley, J., 2005. *Single-crystal X-ray diffraction of spinels from the San Carlos Volcanic Field, Arizona: Spinel as a geothermometer*. American Mineralogist, 90(11–12), pp. 1900–1908.

Wilshire, H.G., Meyer, C.E., Nakata, J.K., Calk, L.C., Shervais, J.W., Nielson, J.E., Schwarzman, E.C., 1988. Mafic and ultramafic xenoliths from volcanic rocks of the western United States. USGS Professional Paper 1443, 179 p.